Published in final edited form as:
Microelectron Eng. 2018 ; 187-188: .

Optical fiber Fabry-Pérot micro-displacement sensor for MEMS in-plane motion stage

Yong-Sik Kim[a], **Nicholas G. Dagalakis**[a], **Young-Man Choi**[b,*]

[a]Intelligent Systems Division, Engineering Laboratory, National Institute of Standards and Technology, 100 Bureau Dr., Gaithersburg, MD 20899, USA

[b]Department of Mechanical Engineering, Ajou University, Suwon 16499, Republic of Korea

Abstract

Fabry-Pérot interferometer sensors have been widely used in Micro-Electro-Mechanical-Systems (MEMS) due to high displacement accuracy and immunity to electromagnetic noises, but they are still limited by micro scale measurement range. In this paper, a Fabry-Pérot interferometer in-plane displacement sensor is proposed for measuring the displacement of MEMS devices utilizing a polished optical fiber and a modulated laser source. The polished optical fiber and a sidewall of a MEMS device form an optical cavity for the proposed sensor. The sinusoidal phase modulation with extreme point search algorithm enables the proposed sensor to measure displacements larger than the wavelengths of the laser light in real time. The experimental results show that the proposed displacement sensor has a capability to measure displacements larger than 3 μm and it shows the measurement accuracy less than 35 nm. The proposed displacement sensor is then embedded on a single degree-of-freedom MEMS motion stage and tested to monitor its displacement in real time.

Keywords

Fabry-Pérot interferometry; Distributed feedback laser; Phase lock; Sinusoidal phase modulation; MEMS; Optical fiber; Displacement sensor

1. Introduction

Micro-Electro-Mechanical Systems (MEMS) have been used in various applications. Among them, miniaturized actuators or motion stages are commonly utilized in space-restricted applications like metrology in a vacuum chamber [1], and handling micro-scale objects for assembly or manipulation [2,3]. Contrary to actuators, the dedicated MEMS displacement sensors for them are still limited, because it is not always easy to miniaturize sensors in micro-scale and to reduce unexpected side effects without sacrificing the performance equivalent to that of macro-scale sensors. Due to this scale difference, some MEMS displacement sensors show high accuracy but provide short range of detection or more fabrication effort.

*Corresponding author. ymanchoi@ajou.ac.kr (Y.-M. Choi).

Dedicated MEMS displacement sensors are designed to monitor movable MEMS components based on relevant principles such as capacitance [4–6], electromagnetics [7], photodiode-based [8], and laser or optics [9]. Depending on sensing mechanisms in micro-scale, each MEMS sensor has its own advantage and disadvantages over the others. Capacitive sensors measure a physical gap by monitoring the change in the capacitance between two electrodes and convert it into displacement information [5]. Though capacitive sensors can provide nanometer level accuracy, they require adequate electrode area because their performance is proportional to the area size of the electrodes [7]. Electromagnetic sensors detect the intensity change of an electric current induced by a magnetic field [7], and it is necessary to get good electric shields around the engaged sensors to avoid any interference with adjacent MEMS components operated by electric signals. Laser or optics-based displacement sensors utilize various approaches such as intensity-based detection [8], fiber Bragg gratings (FBGs) [10], and Fabry-Pérot interferometers (FPIs) [9,11]. An intensity-based optical displacement sensor measures the intensity change of detected light and converts it into displacement information. Beyaz et al. places a MEMS object to measure between a light source and photo detector (PD) [8]. When the MEMS object is in motion, its shadow in front of the PD also changes, resulting in the intensity change of the detected light. This approach is robust to electric noise and can provide a relatively long range of detection of 4 mm. But the resolution of the intensity-based detection is 120 μm, since the intensity-based detection is vulnerable at the stability of laser diode (LD) and the surface condition of mirrors. The FBS method uses a periodic index modulation inside an optical fiber or an optical path embedded on the MEMS device. When a fiber is under stress or strain, the optical fiber will be stretched out or compressed. This change can be converted into a wavelength change with the fiber Bragg grating method [10]. However, this approach requires a spectrum analyzer to monitor the change of the wavelength and the implementation of a corresponding waveguide MEMS fabrication process is more complex than the fabrication of the MEMS object to be measured in general [12].

The Fabry-Pérot interferometers have been widely used for their high sensitivity, low cost, simple structure, and immunity to electromagnetic interference (EMI) [9,11–13]. The FPI utilizes the interference occurring through an optical cavity formed by two separate mirrors [14]. These two reflected streams of light form interference depending on their wavelength and cavity length. In this case, the intensity of the interferometric signal can be expressed as:

$$S(t) = S_{dc} + S_a \cos\frac{k\Delta L}{\lambda} \quad (1)$$

where S_{dc} is the direct current (DC) term of the interferometric signal, S_a is the amplitude of the interference signal, ΔL is the distance change, λ is the wavelength of the light from a laser diode (LD), and k is coefficient depending on the optical path setting. Eq. (1) indicates that the cosine function alone is not enough to figure out whether the motion is forward or backward when the phase shift occurs (or the phase is an integer multiple of $\pi/2$). In this case, additional features are required to measure displacement larger than the half or a quarter of the wavelength of the engaged light. Considering the facts that the wavelength of typical LD varies from 400 nm to 1550 nm and many MEMS actuators can generate displacement larger than a few μm, there is an obvious need to enhance MEMS displacement

sensors for a longer detectable range without sacrificing other advantages. Conventional interferometers utilize additional components or optical set-ups to overcome this limit; One approach is a two wavelengths interferometer using two different LDs [15], which compares two interferometric signals to detect phase shift and determine its motion direction. Another approach is to control the optical path by keeping a phase shift from occurring. In this case, the displacement information can be extracted from the optical path controller [9]. However, it is not easy to implement the components described above through MEMS fabrication processes due to the scale difference. Instead, phase modulation may be used without adding hardware components. The phase modulation adds extra information onto a reference signal [16]. By demodulating the interferometric signal, the sensor can detect the phase shift and its direction of motion. Moreover, it can compensate the intensity fluctuation for better accuracy.

In this paper, a MEMS-embedded Fabry-Pérot interferometric sensor is proposed to measure in-plane displacement of a MEMS device. The MEMS device is specially designed for embedding the FPI sensor. The sidewall of a MEMS moving device and an optical fiber provide the optical cavity for the FPI sensor. The proposed sensor is implemented based on a Fabry-Pérot interferometer and a sinusoidal phase modulation (SPM) to measure a displacement larger than the wavelength of the LD used in the system. Without additional hardware components, a simple algorithm called extreme point search algorithm is proposed for real-time displacement calculation. Finally, we verified the performance of the proposed sensor using reference step-heights and demonstrated its application to the MEMS motion stage.

2. Optical fiber Fabry-Pérot interferometer

2.1. Working principle

The schematic diagram of the proposed FPI sensor is depicted in Fig. 1. This system is based on an extrinsic FPI and enhanced with several features. This system is composed of a laser diode (LD), optical fibers, a 2 × 2 coupler, and a photo-detector (PD) (DET10C[1], Thorlabs [17]). The 2 × 2 coupler in the FPI sensor is connected to a LD (optical fiber 1) and a PD (optical fiber 2). With this set-up, the optical fiber 3 is connected to the polished optical fiber. Some portion of the laser light from the optical fiber 3 is reflected from the end surface of the polished optical fiber marked by A and the other is reflected from the sidewall of the MEMS device marked by B. The reflected lights marked by A and B form an interferometric signal containing distance information at the PD.

The LD used for this system is a wavelength distributed feedback (DFB)-LD [19]. Conventional LDs use two discrete mirrors to generate a laser beam, but the wavelength DFB-LD has lateral metal Bragg gratings or other periodic structures inside itself. With this feature, the wavelength DFB-LD can generate a laser light with a higher Q-factor, which is appropriate for long-distance communication [20]. In addition to this feature, this internal

[1]Certain commercial equipment is identified in this paper to adequately describe the experimental procedure. Such identification does not imply recommendation or endorsement by the National Institute of Standards and Technology nor does it imply that the equipment identified is necessarily the best available for the purpose.

grating structure can be expanded thermally by the injection current. This thermal expansion results in changes in its wavelength [20] and then affects its phase [21]. In this study, this phase change is utilized to detect its phase shift and get better accuracy, called a sinusoidal phase modulation [21,22].

With the set-up described in Fig. 1, the expected interferometric signals are explained here as follows. The injection current generated by the LD controller is in sinusoidal form and can be expressed as:

$$i_a(t) = I_0 + m\ \cos(\omega_c t) \tag{2}$$

where $i_a(t)$ is the electric current from the LD controller, I_0 is the direct current (DC) component of the injection current, m is the amplitude of the alternating current (AC) component of the injection current, and ω_c is the sinusoidal modulation of the angular frequency. Then, the wavelength of the laser light is modulated by the injection current and the interferometric signal detected at the PD can be expressed as:

$$S(t) = S_{dc} + S_a\ \cos\{Z\ \cos(\omega_c t) + \alpha(t)\} \tag{3}$$

where Z is the modulation amplitude, and α is the modulation phase. The term Z and α can be expressed [22] as:

$$Z = \frac{4\pi m \beta L}{\lambda_0^2},\ \ \alpha = \frac{4\pi L}{\lambda_0} \tag{4}$$

where β is the modulation efficiency, λ_0 is the central wavelength of the LD, and L is the distance to measure. Eq. (3) can be expanded in Taylor series, but this series is too complex to solve in real time. Thus, the modulation amplitude Z is adjusted by the injection current to make the whole calculation fast [23], which is explained in the next section.

2.2. Extreme point search algorithm

Fig. 2 shows the expected interferometric signals depending on various values of Z with regard to the reference signal $Z\cos(\omega t)$. With $Z = \pi/2$, the expected interferometric signal looks like a distorted cosine function. As the value of Z varies, one local maximum in the left half side tends to increase and one local minimum in right half side decreases, as shown in Fig. 2(b) and Fig. 2(c). With $Z = \pi$, the local maximum in the left half has a value equal to that of the local minimum in the right half, which is marked by the red dotted line in Fig. 2(d). Since it is easier to check if two values are the same rather than to calculate the difference between the local maximum and minimum, the injection current is controlled to maintain Z equal to π for the real-time calculation of Eq. (3) [23]. To control the injection current for Z equal to π, previous studies extract the time information from the reference signal (the black dashed line in Fig. 2(d)). Then, based on one and half cycle of the inject current, certain samples are extracted from the interferometric signal (the blue solid line in Fig. 2(d)) for the displacement calculation [22,23]. In this case, an additional component is required to monitor the reference signal and the synchronization between the two signals becomes important.

In this study, we used only the interferometric signal to extract meaningful samples for calculating displacement by searching for the extreme points; local minimum, local maximum, global minimum, and global maximum in real-time. To find extrema points, the slope and slop change of the interferometric signal are monitored in real-time by comparing the current interferometric signal with a previous one based on time information. When the target moves, the interferometric signal in Fig. 2(d) can change to either Fig. 2(e) or Fig. 2(f) depending on the magnitude and direction of the displacement of the object. The magnitude of global extrema remains the same but their time information with regard to the reference signal varies. Meanwhile, the magnitude of the local extrema changes, but its time information with regard to the reference signal remains the same. With these features, the extreme points can be identified easily as either local or global by comparing their values with the previous ones. The found extreme points will be utilized to extract the displacement information which is explained in the following section.

2.3. Displacement calculation

To calculate the modulation phase α, five equations can be extracted from Eq. (3) at five different time stamps from A_0 to A_4, which can be expressed [22] as:

$$S_0 = S_{dc} + S_a \cos\alpha \tag{5}$$

$$S_1 = S_{dc} + S_a \cos(Z/2 + \alpha) \tag{6}$$

$$S_2 = S_{dc} + S_a \cos(Z + \alpha) \tag{7}$$

$$S_3 = S_{dc} + S_a \cos(-Z/2 + \alpha) \tag{8}$$

$$S_4 = S_{dc} + S_a \cos(-Z + \alpha) \tag{9}$$

Once the Z value is well controlled to be π [23], the value of S_2 is equal to that of S_4 as shown in Fig. 2(d). Fig. 3 presents an example in that case. From the extreme point search algorithm discussed in the previous section, it is possible to find the values of S_2 and S_4 and its corresponding time stamps, A_2 and A_4. Then, the values of S_0, S_1, and S_3 are calculated from the interferometric signal at another three time stamps of A_0, A_1, and A_3.

The difference between S_2 and S_4 can be extracted from Eqs. (7) and (9) and expressed as:

$$S_4 - S_2 = 2S_a \sin\alpha \sin Z \tag{10}$$

Since the value of S_2 is equal to S_4, the right term in Eq. (10) should be zero and then the value of Z should be preferably equal to π, based on the interferometric signal plotted in Fig. 3. From Eq. (5) to Eq. (8), the displacement L can also be expressed as:

$$L = \frac{\lambda_0}{4\pi}\alpha = \frac{\lambda_0}{4\pi}\tan^{-1}\left(\frac{S_3 - S_1}{S_0 - S_2}\right) \quad (11)$$

Eq. (11) indicates that the displacement information can be extracted based on five sampled points from S_0 to S_4, which is straightforward and is fast enough for real-time measurement.

3. Performance evaluation

The proposed FPI sensor is implemented based on the schematic diagram in Fig. 1. The DFB-LD adapted in this system is PL15J0011FAA-0–1-01[1],[2] with the wavelength of 1550 nm [19]. The injection current to the LD ranges from 10 mA to 100 mA, depending on the installation of the polished optical fiber, with the modulation frequency of 1 kHz. All data detected from the PD are acquired by a personal computer (PC) through a data acquisition board (PCI-6281[1], National Instruments) with a sampling rate of 100 kHz. The extreme point search algorithm and displacement calculation based on Eq. (11) are implemented by LabVIEW[1] software with 250 samples per second.

3.1. Basic performances of the proposed sensor

For the current set-up, the modulation coefficient (β) of the wavelength DFB LD was measured as 0.0184 nm/mA for the injection current of the LD ranging from 20 mA to 50 mA. With this configuration, Eq. (4) indicates that the optical cavity (the distance from point A to point B in Fig. 2) needs to be between 55 mm and 65 mm to make Z equal to π. The LDs with larger injection current can reduce this total distance range requirement, but the low stability of the high power laser may deteriorate the performance of the sensor, and additional equipment is also required for safety reasons. Considering these factors, the polished optical fiber is used with a low power LD to reject beam reflection at the end of the optical fiber. With this set-up, the DC offset and the amplitude of the injection current are utilized to get the desirable interferometric signal plotted in Fig. 3.

To show the effectiveness of the proposed sensor, we evaluated three specifications: the minimum detectable displacement, maximum range and accuracy. First, the minimum detectable displacement of the sensor can be determined by the sensor noise. By measuring the displacement of a fixed mirror target, the sensor noise of 4.6 nm (RMS) is obtained. The electric noise, A/D quantization error, and the stability of the LD are major limiting factors for the minimum detectable displacement. Next, considering that the wavelength of the DFB LD used in the proposed system ranges from 1447 nm to 1553 nm, the ideal maximum detectable range of the proposed system is about 1.5 mm. However, due to the lack of MEMS device with such a large displacement, the proposed system is also tested with conventional motion stages with the displacements less than 40 μm. Lastly, the accuracy of the proposed FPI sensor is estimated by measuring three different well-known geometries, which are called step-heights. A step-height is a reference block having a rectangular metal film on it, as shown in Fig. 4. The thickness of the metal film is uniform and measured

[2]PL15j0011FAA-0-1-01 is replaced by PL15CD0011FAA-0-1-01 from PD-LD, Inc.

accurately in advance. Three step-heights of 91.3 nm, 181 nm, and 460 nm are attached on a manipulator (PCS-6000, Burleigh[1] [24]) and the proposed FPI sensor scans the surface of the step-height by moving the manipulator. The height is obtained by measuring the distance from the metal film and the distance right next to the metal film. This measurement is repeated 20 times for each step-height. The corresponding results are summarized in Table 1. The intrinsic error of the proposed sensor is 7.6 nm and it tends to increase with the measured distance with the rate of 0.0085 (nm/nm).

3.2. Comparison with a commercial laser interferometer

The proposed FP in-plane micro-displacement sensor is also compared with one commercial interferometer by measuring the displacement of the same object at the same time. A homodyne laser interferometer[1] (RLD10, Renishaw) is selected for this comparison. The two systems measure the distance to one mirror attached on a micro-positioner. By moving the mirror in a sinusoidal motion or triangular motion, the movement is measured by both systems and shown in Fig. 5. The displacement measured by the proposed sensor is plotted in a red dotted line and the data obtained with the commercial interferometer is shown in a solid black line. Compared with the commercial one, the proposed FPI sensor shows a linearity error of less than ±1.2% and a peak-to-peak error of less than 1%.

4. Application to a one degree of freedom MEMS motion stage

4.1. Design

The proposed sensor system is designed to measure in-plane displacement of a movable MEMS device. In this paper, a one degree of freedom (DOF) MEMS in-plane motion stage is selected for its stroke larger than a few μm [25,26]. Bergna et al. [25] reports this MEMS stage is able to generate a displacement larger than 10 μm. The motion stage consists of a thermal actuator, a moving platform, and the linkages between them in symmetric layout as shown in Fig. 6(a). This symmetric design guides the moving platform for one DOF motion along the direction indicated by the red arrow in Fig. 6(a). The original motion stage is slightly modified in this paper to embed a polished optical fiber in the laser displacement sensor. For this purpose, a guiding trench is fabricated right next to the moving platform where a polished optical fiber is placed. This trench has an opening near the moving platform to help a polished optical fiber aim toward the sidewall of the moving platform as shown in Fig. 6(b). Once a polished optical fiber is placed on the guiding trench, an aluminum block is placed on top of it to hold it in its position. The laser light emitted from the polished optical fiber is reflected from the sidewall of the moving platform of the one-DOF MEMS motion stage and returns to the polished optical fiber for the displacement measurement. Based on the reflected laser light, the proposed displacement sensor calculates the displacement of the moving platform.

4.2. Fabrications

The optical cavity (or two separate mirrors) is implemented in various ways in MEMS for FPI sensors. Schröpfer et al. [14] developed a MEMS FPI accelerometer utilizing a sidewall of a suspended silicon block and the cleaved end of an optical fiber as an optical cavity to measure the motion of the suspended silicon block. The sidewall of silicon is implemented

with Potassium hydroxide (KOH) [27] or Bosch[1] Deep Reactive Ion Etching (DRIE) [28] in MEMS, which achieve only limited finesse. Due to this reason, the smooth top surface of a MEMS device [29] is utilized for out-of-plane motion detection or an additional diaphragm [30] is required.

The fabrication of the MEMS motion stage for the FPI sensor follows the silicon-on-insulator multi-user multi-processes (SOI-MUMPs) [31] with an additional etching step. The fabrication steps are described in Fig. 7. For this fabrication, a silicon-on-insulator (SOI) wafer is prepared as a starting material, which is composed of a device layer, a handle layer, and a buried oxide layer (Fig. 7(a)). Its first step is the metal deposition of 25 nm of chrome and 50 nm of gold for electric connections (Fig. 7(b)). The second step prepares the guiding trench for the optical fiber on the device layer by performing deep reactive ion etching (Fig. 7(c)). The third step eliminates the buried oxide layer from the trench area and etches both the main structures of the MEMS device on the device layer and the remaining part of the trench on the supporting layer (Fig. 7(d)). This step is required because the diameter of the polished optical fiber is 125 μm, but the device layer is only 25 μm, so additional etching is needed on the handle layer to align the polished optical fiber along the center of the sidewall of the moving platform. For this purpose, an additional etching is performed for the trench depth of 46.5 μm in the handle layer. After the fabrication of the guiding trench, the remaining fabrication process follows SOI-MUMPs for the device layer and the handle layer etching which is described in Fig. 7(e) to Fig. 7(g). After the fabrication, the proposed FPI sensor is placed on the guiding trench as shown in Fig. 7(h). The distance between the end tip of the polished optical fiber and the sidewall of the MEMS motion stage is adjusted to be about 1 mm. With this set-up, the electrothermal actuator of the MEMS motion stage is electrically connected to a DC power source for its operation.

Based on the fabrication process described above, the one-DOF MEMS motion stage is fabricated as shown in Fig. 8(a). Fig. 8(b) presents a guiding trench near its moving platform. Fig. 8(c) shows the side wall surface of the silicon processed by DRIE. The sidewall made by DRIE has a multiple scallop shape. A polished optical fiber is placed into the guiding trench as presented in Fig. 8(d), where a visible red laser is used and the tip of the fiber is slightly inclined for better visualization. With this installation, the proposed sensor is ready to measure the in-plane displacement of the one-DOF MEMS motion stage.

4.3. Experimental results

Fig. 9(a) shows a triangular motion of the MEMS motion stage with an amplitude of 300 nm and a frequency of 1 Hz generated by a driving voltage with the amplitude of 0.5 V and the offset of 2 V. For this offset and small amplitude, the measured output data shows a straight linear motion. Fig. 9(b) shows the displacement measured when the MEMS motion stage is under a sinusoidal driving voltage with a frequency of 0.2 Hz generated by a driving voltage with the amplitude of 2 V and the DC offset of 2 V. The displacement of the MEMS motion stage is a quadrature curve with the amplitude of 3.2 μm. The sinusoidal motion of the MEMS motion stage is slightly distorted, because the displacement of the electrothermal actuator is proportional to the square of the driving voltage [32].

5. Conclusions

In this paper, an in-plane displacement sensor is proposed for MEMS applications. This sensor is based on an extrinsic Fabry-Pérot interferometer for simple design and acceptable accuracy. This also utilizes a polished optical fiber as an interface for a small MEMS device. The proposed sensor is also enhanced with sinusoidal phase modulation, and the extreme point search algorithm. The reference signal carries additional information by controlling an injection current to the LD. This approach increases the range of the detection. The extreme point search algorithm simplifies the optical set-up and makes the whole calculation process straightforward, which enables real-time processing. The evaluation using the reference heights and commercial interferometric system proves that its intrinsic error is less than tens of nm. Finally, the proposed sensor was applied to a MEMS motion stage to monitor its in-plane displacement successfully.

The large range and high accuracy of the proposed sensor can be used in various MEMS applications such as multi-DOF motion measurement and dynamic analysis. Also, the proposed FPI sensor is immune to any electromagnetic noise, so it works effectively in MEMS applications necessarily exposed to various electric noise. In addition, the proposed sensor can be utilized in measuring the out-of-plane motion of MEMS device with 45° angled polishing at the end tip of the engaged optical fiber [33].

Acknowledgments

The fabrication of the MEMS motion stage was performed in part in the NIST Center for Nanoscale Science and Technology Nano Fabrication Clean Room.

References

[1]. Heckert NA, “An EDA approach to experimental design.”

[2]. Sahu B, Leang KK, Taylor CR, Emerging challenges of microactuators for nanoscale positioning, assembly, and manipulation, J. Manuf. Sci. Eng. 132 (3) (2010) 030917.

[3]. Chowdhury S, et al., Automated cell transport in optical tweezers-assisted microfluidic chambers, IEEE Trans. Autom. Sci. Eng. 10 (4) (10 2013) 980–989.

[4]. Zamurovic SHYSA, Dagalakis NG, Lee RD, Kim YS, Embedded capacitive displacement sensor for nanopositioning applications, Proceedings of the Conference on Precision Electromagnetic Measurements, 2010.

[5]. Chu LL, Gianchandani YB, A micromachined 2D positioner with electrothermal actuation and sub-nanometer capacitive sensing, J. Micromech. Microeng. 13 (2) (2003) 279.

[6]. Wang J, Yang Z, Yan G, Silicon-on-insulator out-of-plane electrostatic actuator with in situ capacitive position sensing, J. MicroNanolithography MEMS MOEMS 11 (3) (2012) (pp. 033006–1).

[7]. Choi Y-M, Gorman JJ, Dagalakis NG, Yang SH, Kim YS, Yoo JM, A high-bandwidth electromagnetic MEMS motion stage for scanning applications, J. Micromech. Microeng. 22 (10) (2012) 105012.

[8]. Beyaz MI, McCarthy M, Ghalichechian N, Ghodssi R, Closed-loop control of a longrange micropositioner using integrated photodiode sensors, Sens. Actuators Phys. 151 (2) (4 2009) 187–194.

[9]. Pang C, Bae H, Gupta A, Bryden K, Yu M, MEMS Fabry-Pérot sensor interrogated by optical system-on-a-chip for simultaneous pressure and temperature sensing, Opt. Express 21 (19) (9 2013) 21829–21839. [PubMed: 24104075]

[10]. Berkoff TA, Kersey AD, Experimental demonstration of a fiber Bragg grating accelerometer, IEEE Photon. Technol. Lett. 8 (12) (12 1996) 1677–1679.

[11]. Li M, Wang M, Li H, Optical MEMS pressure sensor based on Fabry-Pérot interferometry, Opt. Express 14 (4) (2 2006) 1497–1504. [PubMed: 19503474]

[12]. OSA|Highly sensitive compact refractive index sensor based on phase-shifted sidewall Bragg gratings in slot waveguide[Online]. Available: https://www.osapublishing.org/ao/fulltext.cfm?uri=ao-53-1-96&id=276299 [Accessed: 14-Jun-2017].

[13]. Bae H, Yu M, Miniature Fabry-Pérot pressure sensor created by using UV-molding process with an optical fiber based mold, Opt. Express 20 (13) (6 2012) 14573–14583. [PubMed: 22714519]

[14]. Schröpfer G, Elflein W, de Labachelerie M, Porte H, Ballandras S, Lateral optical accelerometer micromachined in (100) silicon with remote readout based on coherence modulation, Sens. Actuators Phys. 68 (1) (6 1998) 344–349.

[15]. Cheng JCWYY, Two-wavelength phase shifting interferometry, Appl. Opt. 23 (24) (1985) 4539.

[16]. Sasaki O, Suzuki T, Interferometric Displacement Sensors Using Sinusoidal Phasemodulation and Optical Fibers, vol. 5633, 2005 120–127.

[17]. DET10C - InGaAs detector, 700–1800 nm, 10 ns rise time, 0.8 mm2, 8–32 Taps[Online]. Available: https://www.thorlabs.com/thorproduct.cfm?partnumber=DET10C.

[18]. Dagalakis NG, Kim Y, Displacement Sensor With Embedded Coherent Electromagnetic Radiation Interferometer for Micro Scale Proximity Measurements, 5 2013.

[19]. PD-LD, “PL13/15 DFB Series Laser Diode Modules.”

[20]. Zeller W, Naehle L, Fuchs P, Gerschuetz F, Hildebrandt L, Koeth J, Lasers DFB, Between 760 nm and 16 μm for sensing applications, Sensors 10 (4) (3 2010) 2492–2510. [PubMed: 22319259]

[21]. Sasaki O, Okazaki H, Sinusoidal phase modulating interferometry for surface profile measurement, Appl. Opt. 25 (18) (1986) 3137–3140. [PubMed: 18235589]

[22]. Sasaki O, Takahashi K, Sinusoidal phase modulating interferometer using optical fibers for displacement measurement, Appl. Opt. 27 (19) (1988) 4139–4142. [PubMed: 20539528]

[23]. Suzuki T, Iwana T, Sasaki O, Modulation-amplitude-locked laser diode interferometry for distance, Measurement 5265 (2004) 120–126.

[24]. seg burleigh pcs 6000 bro pdf free ebook download.

[25]. Bergna S, Gorman JJ, Dagalakis NG, Design and modeling of thermally actuated MEMS nanopositioners, ASME 2005 International Mechanical Engineering Congress and Exposition 2005, pp. 561–568.

[26]. Kim Y-S, Shi H, Dagalakis NG, Gupta SK, Design of a MEMS-based motion stage based on a lever mechanism for generating large displacements and forces, J. Micromech. Microeng. 26 (9) (2016) 095008.

[27]. Jung H, Kim CJ, Kong SH, An optimized MEMS-based electrolytic tilt sensor, Sens. Actuators Phys. 139 (1–2) (9 2007) 23–30.

[28]. “Bosch DRIE process.” US Patent US 20070128875 A1.

[29]. Baglio S, Castorina S, Esteve J, Savalli N, Highly sensitive silicon micro-g accelerometers with optical output, 2004 IEEE International Symposium on Circuits and Systems (IEEE Cat. No.04CH37512), vol. 4, 2004, p. IV–868–71.

[30]. Chou N, Yoo S, Kim S, A largely deformable surface type neural electrode array based on PDMS, IEEE Trans. Neural Syst. Rehabil. Eng. 21 (4) (7 2013) 544–553. [PubMed: 22907973]

[31]. Miller K, Cowen A, Hames G, Hardy B, SOIMUMPs Design Handbook, MEMScAP Inc Durh., 2004

[32]. Kim Y-S, Yoo J-M, Yang SH, Choi YM, Dagalaks NG, Gupta SK, Design, fabrication and testing of a serial kinematic MEMS XY stage for multifinger manipulation, J. Micromech. Microeng. 22 (8) (2012).

[33]. Bae H, et al., Miniature Surface-mountable Fabry–Perot Pressure Sensor Constructed with a 45° Angled Fiber, Optical Society of America, 2010.

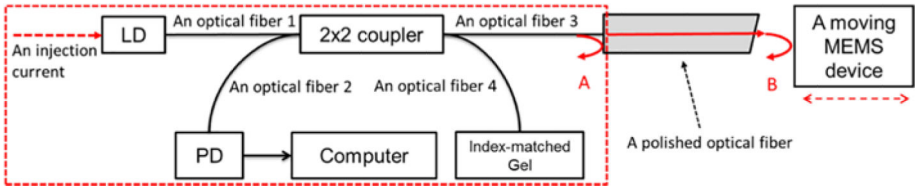

Fig. 1.

A schematic diagram of the proposed FPI displacement sensor [18].

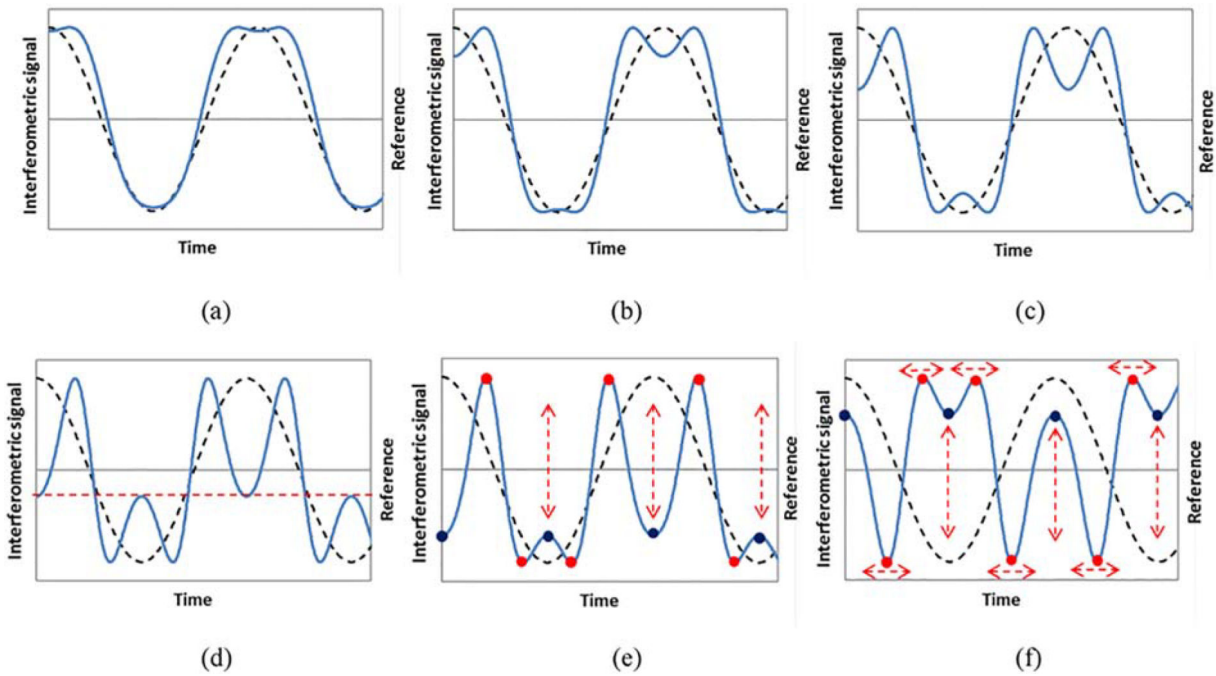

Fig. 2.

The relationship between the interferometric signal in blue solid lines and the reference signal $Z\cos(\omega_c t)$ of Eq. (3) in black dashed line are plotted for; (a) $Z = \pi/2$, (b) $Z = 3\pi/2$, (c) $Z = 3\pi/4$, (d) $Z = \pi$, (e) an interferometric signal changes (shown a red or black points) when the target is in movement, (f) another interferometric signal when the target is in movement. (red dots: global maximum/minimum, black dots: local maximum/minimum).

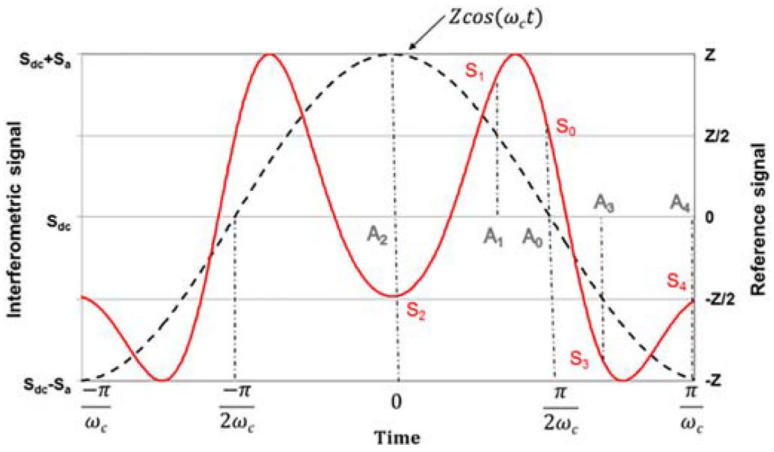

Fig. 3.

The interferometric signal and the reference signal with $Z = \pi$: the reference signal Zcos(wt) in Eq. (3) is plotted with a dashed black line and a corresponding interferometric signal in red solid line. Five important interferometric signal values are marked from S_0 to S_4 and corresponding time stamps indicated from A_0 to A_4.

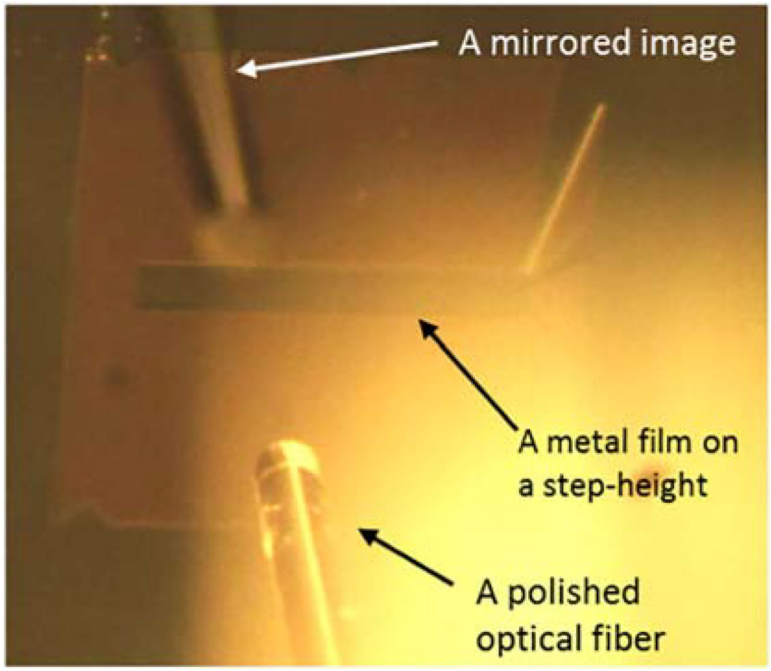

Fig. 4.
Experimental set-up of the proposed FPI sensor for measurement of a step-height.

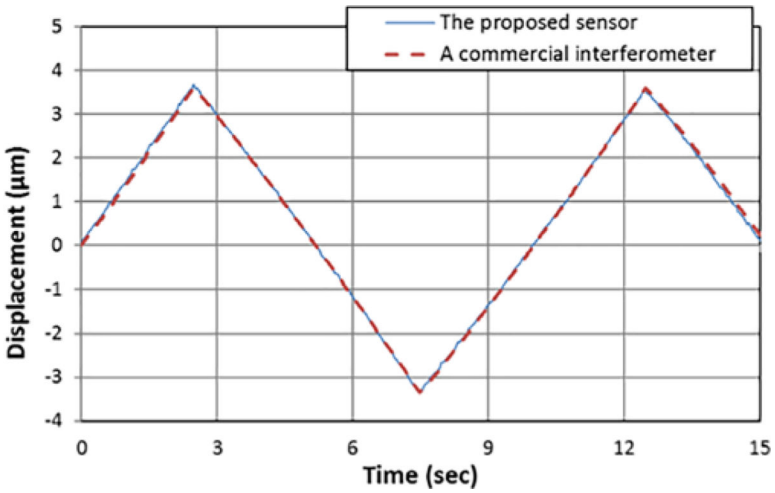

Figure 5.

Comparison of the proposed FPI sensor and the commercial laser interferometer with 0.1 Hz triangular motion of 7 μm stroke.

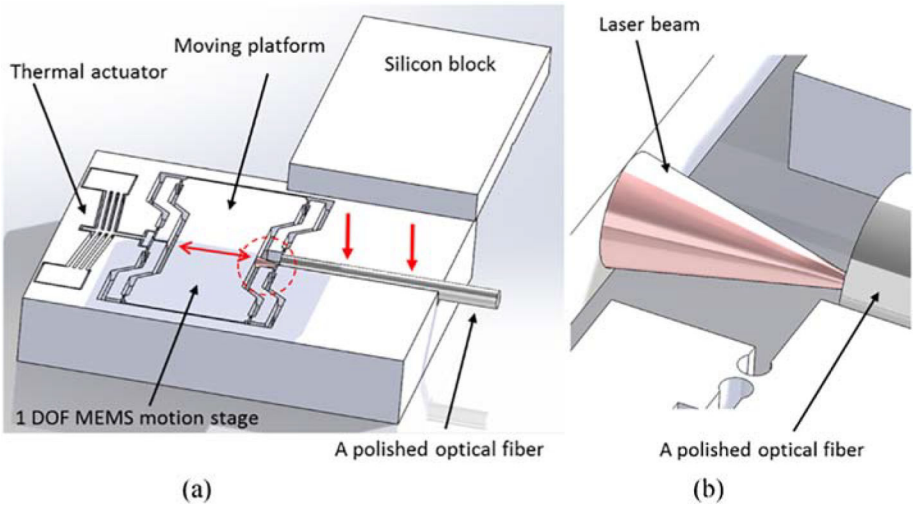

Fig. 6.

The 3D design of the proposed system for MEMS device: (a) overview of the proposed sensor installed on one-DOF MEMS motion stage, (b) the zoomed view of the sidewall of the moving platform circled in (a).

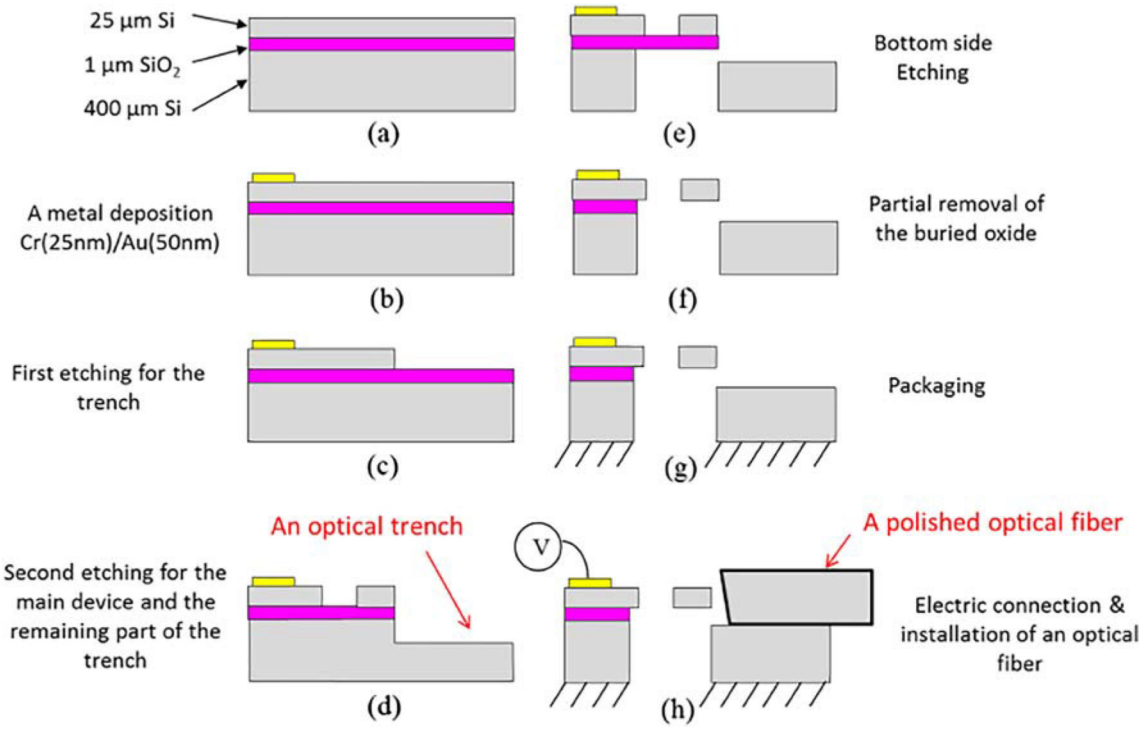

Fig. 7.

MEMS fabrication process based on SOI-MUMPs: (a) SOI wafer; (b) metal pad deposition; (c) first etching for the guiding trench; (d) second etching for the guiding trench and third etching for the main components of the MEMS motion stage; (e) fourth etching of the backside of the motion stage; (f) removal of the buried oxide layer to release the motion stage; (g) packaging or installing on a chip; (h) electrical connection and installation of the optical fiber.

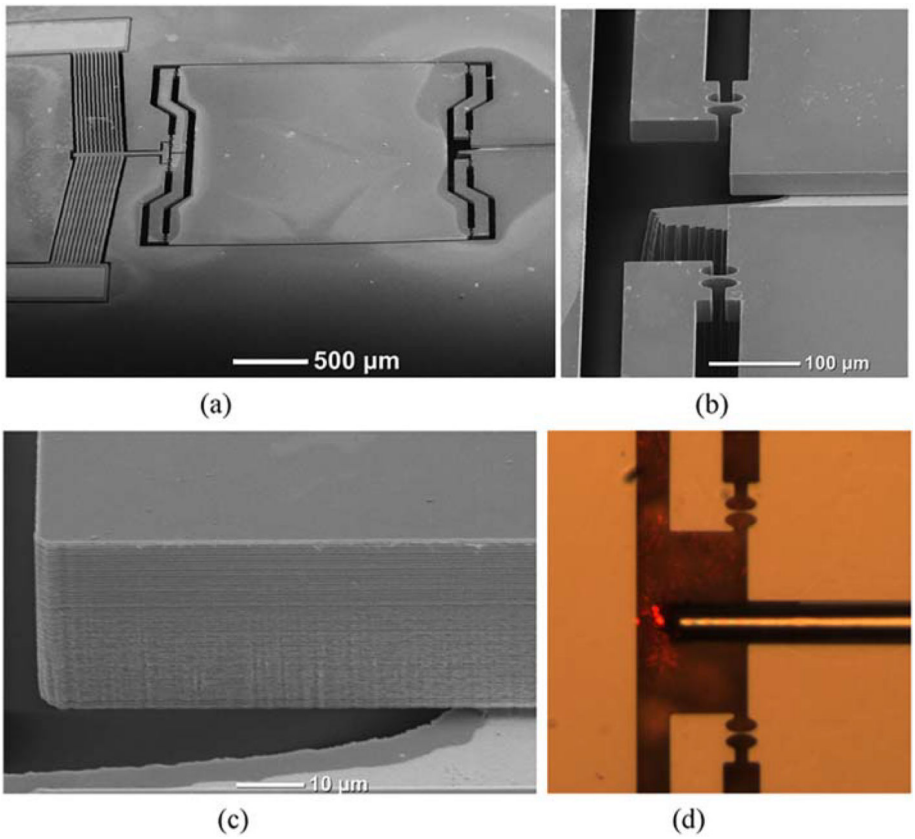

Fig. 8.

A fabricated MEMS motion stage for the proposed FPI sensor: (a) an overall view (SEM image); (b) the guiding trench near the sidewall of the moving platform (SEM image), (c) the surface roughness of the trench sidewall and the top surface (SEM image), and (d) the embedded optical fiber on the guiding trench (optical image).

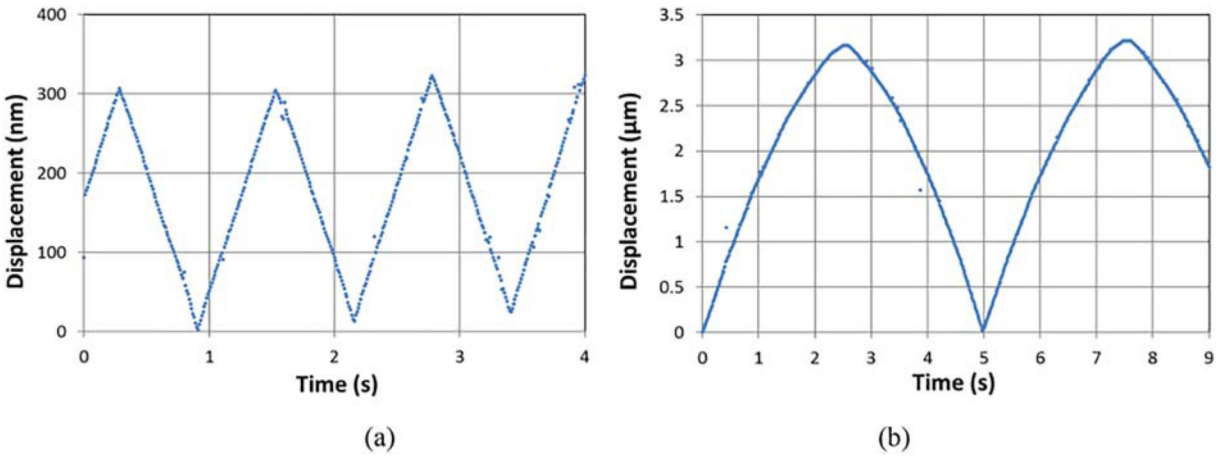

Fig. 9.

Experimental observations of the motions of a MEMS motion stage: (a) the measured displacements of a 1 Hz triangular motion, and (b) the measured displacements of a 0.2 Hz sinusoidal motion.

Table 1

Measurement results of the proposed FPI sensor for three step-heights.

Step heights (nm)	91.3	181	460
Average (nm)	99.7	190.1	471.5
Error (nm)	+8.4	+9.1	+11.5